Materials Science in Semiconductor Processing 172 (2024) 108057

Contents lists available at ScienceDirect

Materials Science in Semiconductor Processing

journal homepage: www.elsevier.com/locate/mssp

Utilizing direct Zener tunneling in Germanium for cryogenic quantum applications

Michael Hack [a,*], Lukas Seidel [a], Maurice Wanitzek [a], Michael Oehme [a], Jörg Schulze [b], Daniel Schwarz [a]

[a] Institute of Semiconductor Engineering (IHT), University of Stuttgart, Pfaffenwaldring 47, Stuttgart, 70569, Germany
[b] Chair of Electron Devices (LEB), Friedrich-Alexander-Universität Erlangen-Nürnberg, Cauerstr. 6, Erlangen, 91058, Germany

ARTICLE INFO

Keywords:
Silicon photonics
Photonic integrated circuit
Quantum applications
Quantum photonic integrated circuit

ABSTRACT

The temperature-dependent electroluminescent properties of Ge-Diodes, especially the Ge-Zener-Emitter, with tunnel transitions are investigated. The direct band-gap behavior of Germanium below a temperature of 140 K is demonstrated, facilitated by Zener tunneling. Pulsed excitation of the Ge-Zener-Emitter results in an optical output power density of 6 μW, which is sufficient to excite quantum dots for single-photon emission. The peak energy of 0.86 eV suits the non-resonant excitation of InGaAs quantum dots at cryogenic temperatures. This paper presents a potential optical pump source for a quantum photonic integrated circuit.

1. Introduction

The need for a stable platform to build functional prototypes for testing the performance and feasibility of quantum sensors, quantum computers, and other quantum applications is rising exponentially. One possibility for such a system is the material Si. This platform has been highly investigated for many years and is well-known in the industry for integrated circuits. The Si system also provides the opportunity to build photonic integrated circuits (PIC), and this technology has made significant progress in the last few years [1–3]. The properties of light can be harnessed for quantum applications, and this knowledge can be integrated with PICs, single-photon sources, and single-photon detectors. Such an integrated system creates the opportunity to build a quantum photonic integrated circuit (QPIC) [4]. As single-photon sources on a QPIC operate in a cryogenic environment, the integrated optical sources also have to function at such temperatures [5]. Due to the low temperature and thus a lack of phonons, the indirect band-gap materials, Si and Ge, lose their light emission efficiency. To achieve direct band-gap behavior and to prevent this efficiency loss, the following two approaches can be used in combination with Ge. In the first approach, the energy difference between the direct (Γ-Valley) and indirect (L-Valley) conduction band (CB) is lowered until the direct CB is below the indirect CB, resulting in a direct band-gap material. This can be achieved either by introducing tensile strain in combination with high n-type doping [6,7] or by using the alloy semiconductor GeSn [8,9]. The second approach is to inject electrons into the direct CB. This can be done by band-to-band tunneling (BTBT) from the valence band (VB) into the direct CB [10]. This second method will be described and investigated in this paper.

2. Materials and methods

The investigated devices are grown on p^- Si (100) substrates with a 6-inch molecular beam epitaxy system. To grow relaxed Ge on Si with a low threading dislocation density, the first 100 nm of Ge are grown as virtual substrate. This virtual substrate is annealed at a high temperature, as described in Ref. [11]. The other active layers are grown after cooling down to growth temperature, as described in Table 1. To keep the doping transition of the PN tunnel junction as sharp as possible, the temperature during the fabrication process is kept below 250 °C. Structuring of the mesa, the oxide windows, and the metallization is initiated by contact lithography using the i-line of an Hg-vapor lamp. The structure of the mesa and metallization is done via inductively coupled plasma reactive ion-etching with HBr as the process gas. As passivation, a SiO_2 layer is deposited via plasma-enhanced chemical vapor deposition. The oxide windows are opened with a reactive ion etching process using CHF_3 as the process gas, followed by a buffered HF etch. For the metallization, sputtered Al is used. The device geometry is illustrated in Fig. 1(a). The width w and the length L used in this paper are $w = 1.6$ μm and $L = 560$ μm.

To enable the possibility of picking up the optical signal from the

* Corresponding author.
E-mail address: michael.hack@iht.uni-stuttgart.de (M. Hack).

https://doi.org/10.1016/j.mssp.2023.108057
Received 5 October 2023; Received in revised form 8 December 2023; Accepted 11 December 2023
Available online 16 December 2023
1369-8001/© 2023 The Authors. Published by Elsevier Ltd. This is an open access article under the CC BY-NC-ND license (http://creativecommons.org/licenses/by-nc-nd/4.0/).

fabricated devices without destroying the optical active interface, the samples undergo a specialized dicing process. During this process, the samples are sawed from the back side, leaving a protective depth of 100 μm. Subsequently, the samples are cleaved with tweezers. An illustration of such a cleaved device can be seen in Fig. 1. The scanning electron microscope (SEM) photo of sample 1, Fig. 1 (b), shows a clean break through the mesa structure. In Fig. 1 (c), the full device structure is shown. At the bottom of Fig. 1(c), the rough interface due to the described dicing process can be observed.

The electroluminescent (EL) signal of the devices is picked up with a multimode fiber, FT300EMT from Thorlabs, and coupled to another multimode bundle, P100-2-VIS-NIR from Ocean Optics, which is connected to the spectrometer, NIRquest-512-2.5 from Ocean Optics. For the electrical continuous wave (CW) excitation, the source measurement unit, 2601A from Keithley, is used. For the pulsed electrical excitation, a pulse generator, PLCS-21 from PicoLAS, in combination with a laser driver, LDP-V 03–100 V4.0 from PicoLAS, is employed. For the temperature-dependent EL measurements, a closed-loop helium cryostat system is employed. The cooling system contains a coldhead, Coolpower 12/45 from Leybold, and a compressor, Coolpak 4000 from Leybold. An illustration of the complete measurement setup is provided in Fig. 2.

To calibrate the system and the optical measurement, a calibrated tungsten halogen light source, HL-3 plus-Cal-EXT from Ocean Optics, is employed. The spectrum of the calibration lamp is measured with the spectrometer, and a transfer function is calculated, assuming that the measured counts are linearly dependent on the optical intensity of the measured signal. The transfer function is used to calculate the optical power density presented in this paper. To estimate the optical power density for pulsed measurements, the transfer function requires further modification. With the presented measurement setup and the used spectrometer, we can only measure the average optical power density. To measure the optical power density during pulsed operation, we need to divide the transfer function by the duty cycle D. To reduce noise and improve the sensitivity of the used spectrometer, the same measurement was performed multiple times, and the average value was utilized. For the CW excitation, an average of 2000 measurements is presented, and for the pulsed excitation, an average of 10 measurements is shown. For both measurements, the integration time of the spectrometer is set to 100 ms.

The electroluminescence of the devices investigated in this paper is measured at different operating points for each device. For sample 1, the operating point of the PN junction is in reverse (Zener) and the PIN junction is operated with forward bias. The PN junction and the PIN junction of samples 2 and 3, respectively, are operated with forward bias. Measuring the PN junction of sample 2 with reverse bias (Zener) results in no emission due to the absence of holes in this operating regime.

3. Theory

For indirect semiconductor materials, such as Ge, the emitted optical intensity decreases as the temperature decreases. Most of the light emitted by a Ge-light emitting diode (LED) originates from the scattering of electrons from the indirect CB to the direct CB, as shown in Fig. 3. This

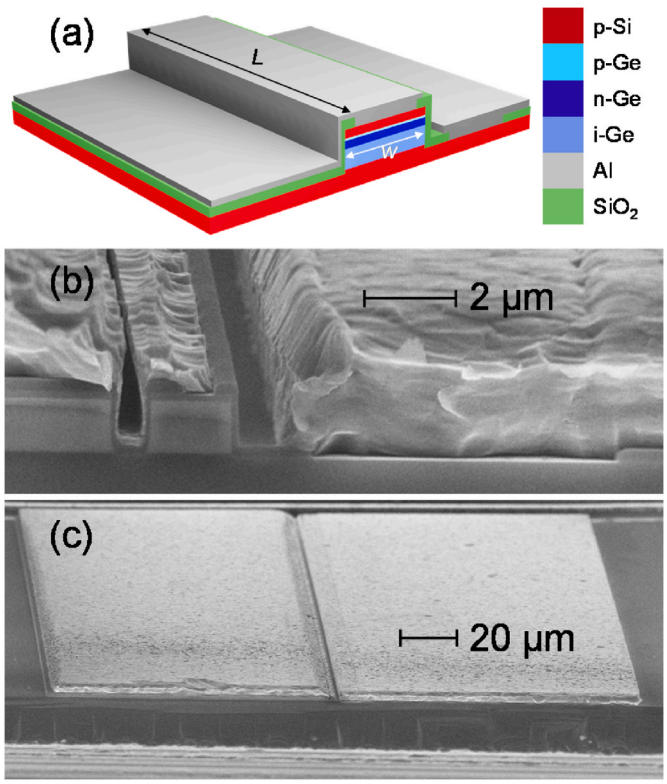

Fig. 1. (a) Device geometry illustration after cleaving the devices (b) Tilted close up SEM photo of the cleaved device (c) Tilted SEM photo of the cleaved device. For both SEM pictures, an EHT voltage of 10 kV and a tilt of 6.9° is used.

scattering mechanism arises from the interaction of charge carriers with lattice phonons. Due to the decrease in phonon density at lower temperatures, the optical intensity also decreases [12,13]. To enhance device performance at low temperatures, an alternative mechanism needs to be used to inject electrons into the direct CB. One possibility is to use the direct BTBT from the VB into the direct CB. For a more detailed description of this effect, see Refs. [14,15]. Particularly high direct BTBT rates can be achieved in Ge PN tunneling junctions compared to Si PN junctions because, at room temperature, the energetic difference between the Γ- and the L- CB in Ge is only 0.136 eV [16]. For radiative recombination, not only electrons in the direct CB are necessary, but also holes need to be present. This is achieved with a PIN structure, where holes drift from the p-side through the intrinsic layer towards the n-side, where the tunnel-injected electrons are in the direct CB. An example of this process can be seen in Fig. 3. For samples 2 and 3, electrons will drift from the n-doped region towards the p-doped region, and holes will drift from the p-doped region towards the n-doped region. For sample 2, due to the low lifetime of carrier minorities, most electrons and holes will recombine near the pn interface. For Sample 3, most electrons and holes will recombine in the intrinsic region.

To use the described device for realizing a QPIC, a closer look at the

Table 1
Layer stacks grown via molecular beam epitaxy.

Sample 1 (PINP)			Sample 2 (PN)			Sample 3 (PIN)		
Thickness	Material	Doping (cm^{-3})	Thickness	Material	Doping (cm^{-3})	Thickness	Material	Doping (cm^{-3})
200 nm	p-Si	$N_A = 1 \bullet 10^{20}$	100 nm	n-Si	$N_D = 1 \bullet 10^{20}$	100 nm	n-Si	$N_D = 1 \bullet 10^{20}$
50 nm	p-Ge	$N_A = 1 \bullet 10^{20}$	100 nm	n-Ge	$N_D = 1 \bullet 10^{20}$	100 nm	n-Ge	$N_D = 1 \bullet 10^{20}$
200 nm	n-Ge	$N_D = 2 \bullet 10^{19}$	300 nm	n-Ge	$N_D = 3 \bullet 10^{19}$	300 nm	i-Ge	
500 nm	i-Ge		400 nm	p-Ge	$N_A = 1 \bullet 10^{20}$	100 nm	p-Ge	$N_A = 1 \bullet 10^{20}$
400 nm	p-Si	$N_D = 1 \bullet 10^{20}$	50 nm	p-Si	$N_A = 1 \bullet 10^{20}$	400 nm	p-Si	$N_A = 1 \bullet 10^{20}$
Si-Substrate			Si-Substrate			Si-Substrate		

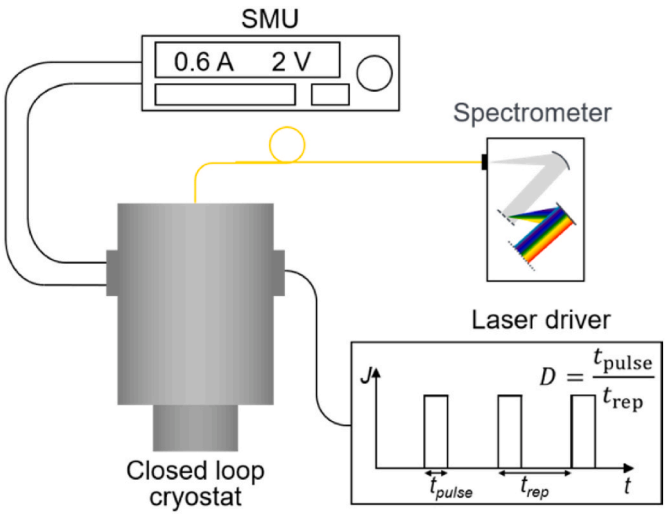

Fig. 2. Measurement setup for cryogenic EL measurements under CW and pulsed excitation.

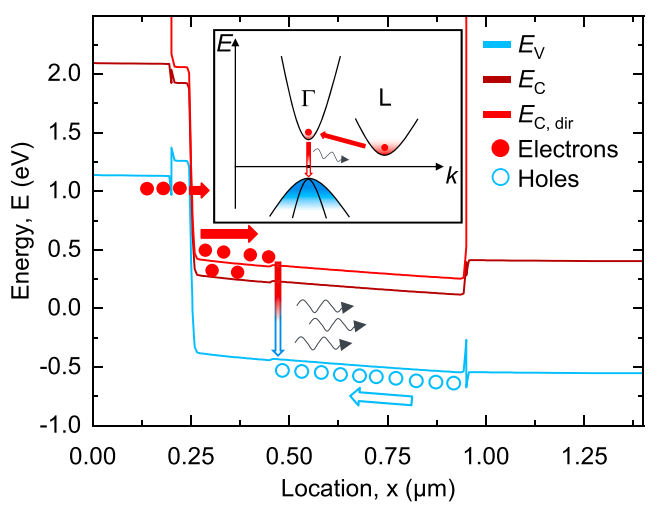

Fig. 3. Band diagram of sample 1 at a voltage of $V = 2$ V. Inset: Simplified band structure of Ge and scattering of electrons from the indirect CB into the direct CB.

single-photon sources will be provided. In current research, GaAs and InGaAs quantum dots (QD) stand among the best single-photon sources available today [4]. Especially for quantum communication, the telecom O- (1.3 μm) and C-Band (1.55 μm) are of special interest. With self-assembled QD on a metamorphic buffer layer, InGaAs QD, emitting single photons in the Telecom C band can be grown. A further description can be found in Ref. [5]. To optically excite these QD, there are two typically used excitation schemes: non-resonant excitation and quasi-resonant or resonant excitation. For non-resonant excitation, an electron-hole pair is generated in the buffer layer (i.e. GaAs), and this electron-hole pair diffuses until it gets trapped inside the QD, relaxing to the lowest energetic state, the s-shell. This excitation scheme is also called above band-gap excitation because the energy of the optical pump source needs to be above the energy level of the buffer layer. For quasi-resonant or resonant excitation, the electron-hole pair is already created inside the QD, and the excitation energy needs to fit the QD energy states [17]. The advantage of non-resonant excitation is that there is no need to separate the emitted light by the pump source and the single photons emitted by the QD. The disadvantage of non-resonant excitation is that, due to the relaxation process, uncertainty is introduced into the emission process. This can increase the time jitter and limits the indistinguishability of the single photons. Another disadvantage of the non-resonant scheme is that electron-hole pairs may also be generated near the QD, resulting in the possibility of electron-electron scattering. This introduces a source of decoherence for subsequently emitted single photons [18]. Despite the disadvantages of the non-resonant excitation scheme, the flexibility in choosing the optical pump source, which only requires above band-gap excitation, facilitates simpler integration for a complete QPIC. The non-resonant excitation scheme can be used as a first demonstrator, and with further band-gap engineering of the optical pump source, resonant excitation could also be possible. The hybrid integration of GaAs QD on the Si platform has already been shown [19]. Also, the fully on-chip integration of InGaAs QD with a single-photon detector has been demonstrated [20]. Therefore, while the integration of QD with a single-photon detector has already been shown, the integration of an integrated optical pump source is still pending.

4. Results and discussion

The electrical characteristics of all three samples are shown in Fig. 4. Sample 1 exhibits the following characteristic behaviors: At Voltages $V < 0$, the sample shows the typical blocking behavior of a PIN diode. Upon closer examination of the voltages between $-0.3 < V < 0$ V, a negative differential resistance (NDR) can be observed, which is strongly limited due to the blocking PIN diode. This NDR exhibits the typical nature of a PN tunnel diode in the Esaki regime. For voltages $V > 0$ V, the typical I(V) characteristic of a Ge PIN diode is evident. Due to the limiting of the PIN diode in sample 1, Zener tunneling cannot be observed in the I(V) curves. Sample 2 displays the temperature-dependent characteristics of a tunneling diode (PN). The NDR is evident in the Esaki regime ($V < 0$), and the Zener tunneling can be observed in the Zener regime ($V > 0$). Sample 3 shows the typical nature of a Ge PIN diode with the temperature-dependent blocking characteristic, attributed to trap states, as described in Ref. [21], and the built-in voltage in the forward direction, which becomes apparent at lower temperatures.

The temperature-dependent emission spectra are presented in Fig. 5. For samples 2 and 3, a decrease in optical power density at lower temperatures can be observed. The optical power density for sample 2 decreases at temperatures ranging from 290 K to 140 K. This behavior of samples 1, 2, and 3 corresponds to the indirect material properties of Ge. Due to the decrease in phonon density, the scattering of electrons from the indirect CB into the direct CB decreases, leading to a decrease in radiative recombination and resulting in a lower optical power density. For sample 1, at temperatures ranging from 140 K to 15 K, the optical power density increases. This can be described by two effects: the direct BTBT and the decrease in scattering from the direct to the indirect CB. For the direct BTBT, the decrease in phonon density leads to a lower parasitic indirect BTBT, resulting in a higher direct BTBT [22]. The injected electrons into the direct CB have to travel through the highly n-doped region before being able to recombine with the holes, leading to radiative recombination. During this time, the electrons can scatter from the direct CB into the indirect CB, leading to a lower electron population of the Γ-Valley in the i-Ge layer. As the phonon density decreases, the effect of scattering can be reduced, leading to a higher electron population of the Γ-Valley. Considering the peak position of the spectra towards lower temperatures, a blue shift can be seen. With the peak position, we estimated the band gap of the material for the different temperatures, as shown in Fig. 6 [23]. The band-gap shift is in good agreement with the temperature-dependent energy band gap of Ge [24].

To confirm that the direct behavior is due to the direct BTBT, the temperature-dependent peak optical power density for all three samples is shown in Fig. 6. For samples 2 and 3, a decrease in the optical power density is observed. This confirms that the direct behavior of sample 1 is the result of the combination of the PN tunnel junction with the PIN

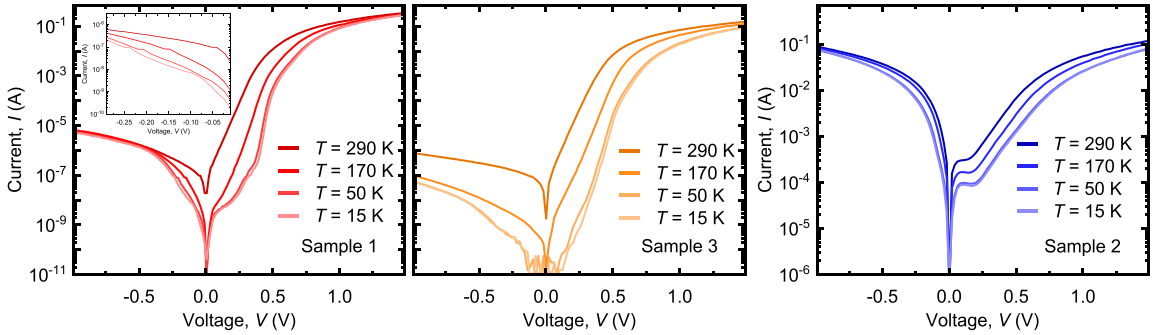

Fig. 4. Temperature-dependent I(V) characteristics of samples 1, 2, and 3. Inset: negative differential resistance of the tunneling diode in the Esaki regime of sample 1. Device area for all three samples: $A = 9 \bullet 10^{-6}$ cm^2.

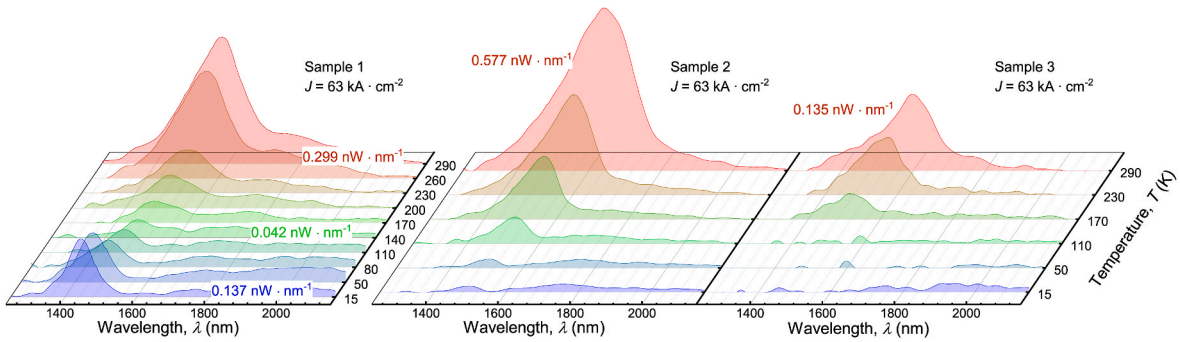

Fig. 5. Temperature-dependent EL emission as a function of wavelength at a current density of $J = 63$ kA cm^{-2}. Voltages at a Temperature of $T = 15$ K: Sample 1 $V_1 = 2$ V, Sample 2 $V_2 = 2.2$ V, Sample 3 $V_3 = 2$ V.

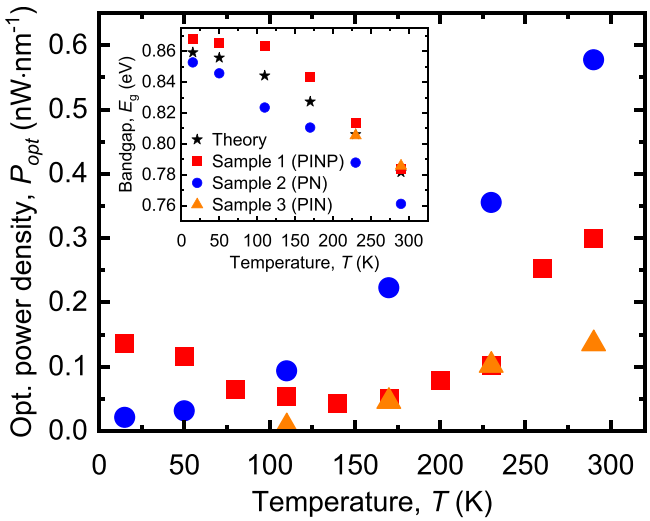

Fig. 6. Temperature-dependent peak optical power density, of the samples discussed in this paper, at a current density of $J = 63$ kA cm^{-2}. Inset: Temperature-dependent shift of the Band gap for Ge and the discussed samples.

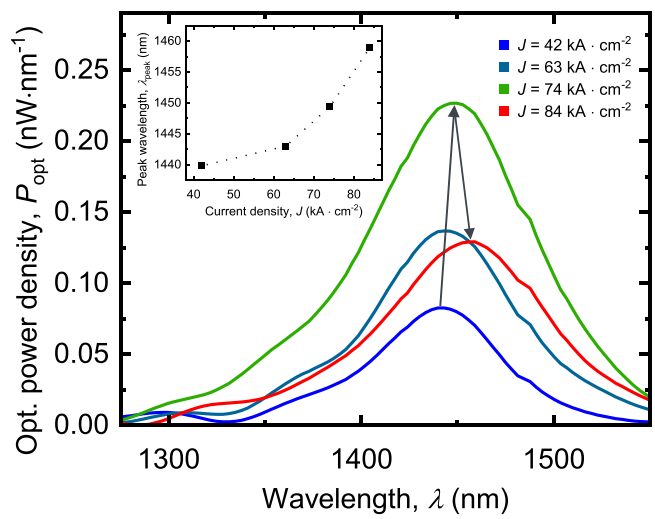

Fig. 7. CW EL measurements of sample 1 at a temperature of 15 K. Inset: Peak wavelength in dependency of the current density.

structure. For comparison, the peak optical power density of Sample 1 is also added to Fig. 6.

In the CW EL measurements for sample 1, at $T = 15$ K, Fig. 7, an increase in the optical power density is observed for low injection powers. However, for current densities above $J > 74$ kA cm^{-2}, a decrease in optical power density is observed. To comprehend the cause of the efficiency drop in the presented device, Fig. 8 provides an overview of possible carrier paths and recombination processes. Considering the dependency on temperature and current density. Fig. 8(c) illustrates the carrier path for radiative recombination, which we aim to maximize and is largely dependent on the other recombination processes. Fig. 8(d) shows Shockley-Read-Hall recombination, primarily influenced by crystal properties rather than current density or temperature. For group III-IV-LEDs a decrease in efficiency at high injection current densities is known as efficiency droop. Potential reasons for the efficiency droop include Joule heating, electron leakage, and Auger recombination [25, 26]. Auger recombination, Fig. 8(e), and the electron leakage, Fig. 8(f), are highly dependent on current density. Additionally, for our device, it is crucial to consider that direct and indirect BTBT are not only

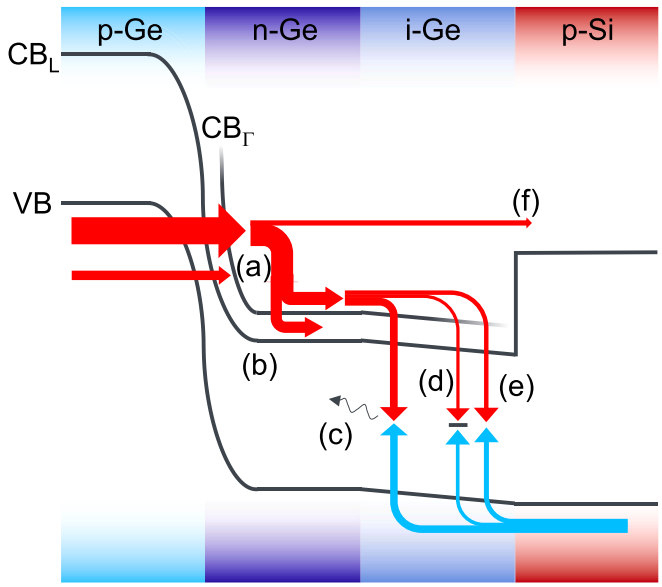

Fig. 8. Possible carrier paths for sample 1 at operating Voltage: (a) Direct and indirect BTBT (b) scattering from direct CB into indirect CB (c) radiative recombination (d) Shockley-Read-Hall recombination (e) Auger recombination (f) electron leakage.

dependent on temperature but also on current density, as shown in Fig. 8 (a) [15,27]. Furthermore, with additional Joule heating, scattering from the direct CB into the indirect CB increases, as shown in Fig. 8(b).

As an indicator for the temperature of the optically active layer, the peak wavelength is used. To extract the thermal shift of the devices, the peak wavelength is plotted over the electrical pump power and linearly extrapolated to the zero point [28]. Contrary to our measurements, see Fig. 7, we do not observe this linear relationship. This is because, at low temperatures, the band gap is not linearly dependent on temperature [24]. It is important to keep this in mind while considering the peak wavelength as an indicator for the temperature of the optically active layer. Therefore, we can only identify if the temperature of the optically active layer is changing, but not quantify the extent of the change. To investigate if the efficiency drop is due to the Joule heating, measurements with pulsed current injections are performed, see Fig. 9. By

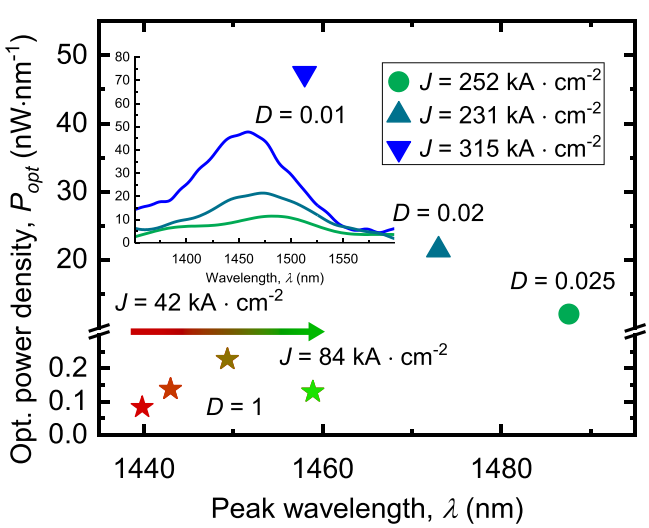

Fig. 9. Peak optical power density in dependency of the peak wavelength as an estimation for the temperature of the optically active layer. CW and pulsed measurements of sample 1 at a temperature of 15 K. Inset: Optical spectra with pulsed excitation.

comparing the same current density at different duty cycles, the effect of the Joule heating can be analyzed. This is because, with lower duty cycles, the injected electrical energy is lower, resulting in a decrease in Joule heating. However, the effects due to current density remain constant. For lower duty cycles, a clear blue shift of the peak wavelength is observed, indicating a lower temperature of the optically active layer. For different current densities and duty cycles, the optical power density is primarily influenced by the duty cycle, resulting in a higher optical power density for lower duty cycles. This indicates that the dominant effect on efficiency lowering for high-current injections is Joule heating. This is most likely due to the higher scattering from the direct CB into the indirect CB, and not due to the still-investigated efficiency droop observed in group III-IV-LEDs.

The maximum possible emitted power of sample 1, at a temperature of $T = 15$ K, pulsed operation with a duty cycle of $D = 0.01$, and a current density of $J = 315$ kA cm^{-2}, is calculated to be $P = 6$ μW. This value is not limited by the device but rather by the measurement setup and the laser driver. Compared with the non-resonant and resonant excitation powers of reported QD operations, a power in the range of nW to μW is needed [29,30]. With the pulsed operation of our device, we have clearly shown that the emitted optical power is sufficient to be used as an integrated optical pump source for cryogenic quantum applications. It is important to differentiate between pulsed electrical excitation of the pump source and pulsed excitation of the QD. With an electrical pulse width of $t_{pulse} = 100$ ns and typical exciton lifetimes in the range of 100 ps to 1 ns, the excitation scheme for the QD needs to be considered as CW excitation [30,31].

As discussed for the first time, we investigated direct and indirect behavior in the same device. Due to the direct behavior at low temperatures, our device needs to be compared with direct-material LEDs. The reason for the efficiency drop of Group III-V-LEDs is still highly discussed. For our device, we have clearly shown that the efficiency lowering is mainly due to Joule heating, but further investigation needs to be performed to determine if this is due to the efficiency droop or due to the scattering characteristics of our device. The optical power of the presented device is enough for the excitation of QDs and can be used as an integrated optical pump source for cryogenic quantum applications. For the realization of a QPIC the transmission of light from our device to the QD needs to be further investigated. Also, the spectral width of the emission line of our device is still quite large. To separate the optical signal of the pump source and the QD, a smaller spectral width of the emission line of the pump source needs to be realized. This can be achieved through the fabrication of distributed Bragg reflectors.

5. Conclusion

We have demonstrated the fabrication and characterization of a Ge-Zener Emitter that utilizes direct BTBT for light emission. Due to the momentum conservation of the tunneling effect, electrons can be injected into the direct CB of Ge. Due to the PIN structure, holes are drifting towards the injected electrons. This enables radiative recombination at cryogenic temperatures. At a temperature of 15 K, an estimated total optical power of 6 μW is achievable with pulsed operation. This shows that monolithic integration of an optical source, operating at cryogenic temperatures, is feasible with Ge on a Si chip. It provides the possibility of an integrated optical pump source for pumping QD and paves the way for a fully integrated QPIC.

CRediT authorship contribution statement

Michael Hack: Writing – review & editing, Writing – original draft, Visualization, Validation, Resources, Methodology, Investigation, Formal analysis, Data curation, Conceptualization. **Lukas Seidel:** Writing – review & editing, Validation, Resources, Conceptualization. **Maurice Wanitzek:** Writing – review & editing, Validation, Resources. **Michael Oehme:** Writing – review & editing, Supervision,

Conceptualization. **Jörg Schulze:** Writing – review & editing, Project administration, Funding acquisition, Conceptualization. **Daniel Schwarz:** Writing – review & editing, Resources, Conceptualization.

Declaration of competing interest

The authors declare that they have no known competing financial interests or personal relationships that could have appeared to influence the work reported in this paper.

Data availability

No data was used for the research described in the article.

Acknowledgements

The authors would like to thank for the funding of this work by the Deutsche Forschungsgemeinschaft (DFG, German Research Foundation) - 431314977/GRK2642

References

[1] X. Wang, J. Liu, Emerging technologies in Si active photonics, J. Semiconduct. 6 (2018), 61001, https://doi.org/10.1088/1674-4926/39/6/061001.
[2] S.Y. Siew, B. Li, F. Gao, H.Y. Zheng, W. Zhang, P. Guo, S.W. Xie, A. Song, B. Dong, L.W. Luo, C. Li, X. Luo, G.-Q. Lo, Review of silicon photonics technology and platform development, J. Lightwave Technol. 13 (2021) 4374–4389, https://doi.org/10.1109/JLT.2021.3066203.
[3] T. Komljenovic, M. Davenport, J. Hulme, A.Y. Liu, C.T. Santis, A. Spott, S. Srinivasan, E.J. Stanton, C. Zhang, J.E. Bowers, Heterogeneous silicon photonic integrated circuits, J. Lightwave Technol. 1 (2016) 20–35, https://doi.org/10.1109/JLT.2015.2465382.
[4] G. Moody, V.J. Sorger, D.J. Blumenthal, P.W. Juodawlkis, W. Loh, C. Sorace-Agaskar, A.E. Jones, K.C. Balram, J.C.F. Matthews, A. Laing, M. Davanco, L. Chang, J.E. Bowers, N. Quack, C. Galland, I. Aharonovich, M.A. Wolff, C. Schuck, N. Sinclair, M. Lončar, T. Komljenovic, D. Weld, S. Mookherjea, S. Buckley, M. Radulaski, S. Reitzenstein, B. Pingault, B. Machielse, D. Mukhopadhyay, A. Akimov, A. Zheltikov, G.S. Agarwal, K. Srinivasan, J. Lu, H.X. Tang, W. Jiang, T. P. McKenna, A.H. Safavi-Naeini, S. Steinhauer, A.W. Elshaari, V. Zwiller, P. S. Davids, N. Martinez, M. Gehl, J. Chiaverini, K.K. Mehta, J. Romero, N. B. Lingaraju, A.M. Weiner, D. Peace, R. Cernansky, M. Lobino, E. Diamanti, L. T. Vidarte, R.M. Camacho, 2022 Roadmap on integrated quantum photonics, J. Phys. Photonics. 1 (2022), 12501, https://doi.org/10.1088/2515-7647/ac1ef4.
[5] C. Carmesin, F. Olbrich, T. Mehrtens, M. Florian, S. Michael, S. Schreier, C. Nawrath, M. Paul, J. Höschele, B. Gerken, J. Kettler, S.L. Portalupi, M. Jetter, P. Michler, A. Rosenauer, F. Jahnke, Structural and optical properties of InAs/(In)GaAs/GaAs quantum dots with single-photon emission in the telecom C-band up to 77 K, Phys. Rev. B 12 (2018), https://doi.org/10.1103/PhysRevB.98.125407.
[6] J. Liu, X. Sun, R. Camacho-Aguilera, L.C. Kimerling, J. Michel, Ge-on-Si laser operating at room temperature, Opt. Lett. 5 (2010) 679–681, https://doi.org/10.1364/OL.35.000679.
[7] R.E. Camacho-Aguilera, Y. Cai, N. Patel, J.T. Bessette, M. Romagnoli, L. C. Kimerling, J. Michel, An electrically pumped germanium laser, Opt Express 10 (2012) 11316–11320, https://doi.org/10.1364/OE.20.011316.
[8] R. Soref, Direct-bandgap compositions of the CSiGeSn group-IV alloy, Opt. Mater. Express 4 (2014) 836, https://doi.org/10.1364/OME.4.000836.
[9] B. Marzban, L. Seidel, T. Liu, K. Wu, V. Kiyek, M.H. Zoellner, Z. Ikonic, J. Schulze, D. Grützmacher, G. Capellini, M. Oehme, J. Witzens, D. Buca, Strain engineered electrically pumped SiGeSn microring lasers on Si, ACS Photonics (2022), https://doi.org/10.1021/acsphotonics.2c01508.
[10] J.V. Morgan, E.O. Kane, Observation of direct tunneling in germanium, Phys. Rev. Lett. 10 (1959) 466–468, https://doi.org/10.1103/PhysRevLett.3.466.
[11] M. Oehme, J. Werner, M. Kaschel, O. Kirfel, E. Kasper, Germanium waveguide photodetectors integrated on silicon with MBE, Thin Solid Films 1 (2008) 137–139, https://doi.org/10.1016/j.tsf.2008.08.062.
[12] N. Tandon, J.D. Albrecht, L.R. Ram-Mohan, Electron-phonon interaction and scattering in Si and Ge: implications for phonon engineering, J. Appl. Phys. 4 (2015), https://doi.org/10.1063/1.4927530.
[13] J. Menéndez, C.D. Poweleit, S.E. Tilton, Temperature-dependent photoluminescence in Ge: experiment and theory, Phys. Rev. B 19 (2020), https://doi.org/10.1103/PhysRevB.101.195204.
[14] R. Koerner, D. Schwaiz, I.A. Fischer, L. Augel, S. Bechler, L. Haenel, et al., The Zener-Emitter: a novel superluminescent Ge optical waveguide-amplifier with 4.7 dB gain at 92 mA based on free-carrier modulation by direct Zener tunneling monolithically integrated on Si, in: 2016 IEEE International Electron Devices Meeting (IEDM). 2016 IEEE International Electron Devices Meeting (IEDM), IEEE, San Francisco, CA, USA, 2016, pp. 22.5.1–22.5.4, 03.12.2016 - 07.12.2016.
[15] K.-H. Kao, A.S. Verhulst, W.G. Vandenberghe, B. Soree, G. Groeseneken, K. de Meyer, Direct and indirect band-to-band tunneling in germanium-based TFETs, IEEE Trans. Electron. Dev. 2 (2012) 292–301, https://doi.org/10.1109/TED.2011.2175228.
[16] O. Madelung, U. Rössler, M. Schulz, Group IV Elements, IV-IV and III-V Compounds. Part B - Electronic, Transport, Optical and Other Properties, Springer-Verlag (b), Berlin/Heidelberg, 2002.
[17] Peter (Hg Michler, Quantum Dots for Quantum Information Technologies, Springer International Publishing (Nano-Optics and Nanophotonics), Cham, 2017.
[18] Simone Luca Portalupi, Peter Michler, Resonantly excited quantum dots: superior non-classical light sources for quantum information, in: Hg Peter Michle (Ed.), Quantum Dots for Quantum Information Technologies, Springer International Publishing (Nano-Optics and Nanophotonics), Cham, 2017, pp. 77–121.
[19] A. Chanana, H. Larocque, R. Moreira, J. Carolan, B. Guha, E.G. Melo, V. Anant, J. Song, D. Englund, D.J. Blumenthal, K. Srinivasan, M. Davanco, Ultra-low loss quantum photonic circuits integrated with single quantum emitters, Nat. Commun. 1 (2022) 7693, https://doi.org/10.1038/s41467-022-35332-z.
[20] M. Schwartz, E. Schmidt, U. Rengstl, F. Hornung, S. Hepp, S.L. Portalupi, K. Llin, M. Jetter, M. Siegel, P. Michler, Fully on-chip single-photon hanbury-Brown and twiss experiment on a monolithic semiconductor-superconductor platform, Nano Lett. 11 (2018) 6892–6897, https://doi.org/10.1021/acs.nanolett.8b02794.
[21] M. Schmid, M. Kaschel, M. Gollhofer, M. Oehme, J. Werner, E. Kasper, J. Schulze, Franz–Keldysh effect of germanium-on-silicon p–i–n diodes within a wide temperature range, Thin Solid Films (2012) 110–114, https://doi.org/10.1016/j.tsf.2012.10.087.
[22] E.O. Kane, Theory of tunneling, J. Appl. Phys. 1 (1961) 83–91, https://doi.org/10.1063/1.1735965.
[23] M. Oehme, M. Gollhofer, D. Widmann, M. Schmid, M. Kaschel, E. Kasper, J. Schulze, Direct bandgap narrowing in Ge LED's on Si substrates, Opt Express 2 (2013) 2206–2211, https://doi.org/10.1364/OE.21.002206.
[24] Y.P. Varshni, Temperature dependence of the energy gap in semiconductors, Physica 1 (1967) 149–154, https://doi.org/10.1016/0031-8914(67)90062-6.
[25] J. Cho, E.F. Schubert, J.K. Kim, Efficiency droop in light-emitting diodes: challenges and countermeasures, Laser Photon. Rev. 3 (2013) 408–421, https://doi.org/10.1002/lpor.201200025.
[26] S. Lin, T. Shih, W. Yan, Y. Lu, Y. Lin, R.R.-G. Chang, Z. Chen, Maximum limits on external quantum efficiencies in bare LEDs, IEEE Trans. Electron. Dev. 4 (2017) 1597–1601, https://doi.org/10.1109/TED.2017.2657553.
[27] E.O. Kane, Zener tunneling in semiconductors, J. Phys. Chem. Solid. 2 (1960) 181–188, https://doi.org/10.1016/0022-3697(60)90035-4.
[28] B. Schwartz, A. Klossek, M. Kittler, M. Oehme, E. Kasper, J. Schulze, Electroluminescence of germanium LEDs on silicon: influence of antimony doping, Phys. Status Solidi C 11–12 (2014) 1686–1691, https://doi.org/10.1002/pssc.201400056.
[29] S. Münch, S. Reitzenstein, P. Franeck, A. Löffler, T. Heindel, S. Höfling, L. Worschech, A. Forchel, The role of optical excitation power on the emission spectra of a strongly coupled quantum dot-micropillar system, Opt Express 15 (2009) 12821–12828, https://doi.org/10.1364/OE.17.012821.
[30] A. Dousse, J. Suffczyński, A. Beveratos, O. Krebs, A. Lemaître, I. Sagnes, J. Bloch, P. Voisin, P. Senellart, Ultrabright source of entangled photon pairs, Nature 7303 (2010) 217–220, https://doi.org/10.1038/nature09148.
[31] S. Hepp, M. Jetter, S.L. Portalupi, P. Michler, Semiconductor quantum dots for integrated quantum photonics, Adv. Quantum Tech. 9 (2019), 1900020, https://doi.org/10.1002/qute.201900020.